Probabilistic Wind Uplift Resistance Framework for the Relative Evaluation of Wood-Frame Load Paths

Brandon M. Rittelmeyer [Corresponding Author]

Ph.D. Candidate
Department of Civil and Environmental Engineering
Auburn University
238 Harbert Center, 205 W. Magnolia Avenue
Auburn, Alabama 36849, United States
Email: bmr0036@auburn.edu

David B. Roueche, Ph.D.

Associate Professor
Department of Civil and Environmental Engineering
Auburn University
234 Harbert Center, 205 W. Magnolia Avenue
Auburn, Alabama 36849, United States
Email: dbroueche@auburn.edu

Keywords:

Probabilistic Analysis Residential Construction Wind Resistance Wood-Frame Load Path

Abstract

Past failure risk analyses of wind-impacted wood-frame structural load paths have tended to consider simplified resistance models that account for a few key load path connections, in which connection capacity distributions are generally based on benchmark experimental results. However, recent post-storm reconnaissance studies have demonstrated that connections in the load path of light wood-frame structures are themselves composed of multiple elements with many configurations and possible failure modes. This study presents a flexible approach for modeling wind uplift resistance in wood-frame load paths that includes a more exhaustive set of potential failure points yet is computationally efficient and readily adaptable to various load paths composed of different assemblages of structural members and connections. In this framework, ultimate capacities of connections and wood members are either based on design equations provided in the National Design Specification for Wood Construction or another applicable standard or computed from a comparable mechanics-based model. Analytical capacity estimates for roof sheathing, roofto-wall connections, and wall-to-slab-foundation connections accord well with the range of published experimental results for these connections. Capacities of connections that act in parallel are summed to transform the load path into an analogous load chain of series components. Systemlevel wind uplift resistance, defined by the weakest component in series, is evaluated by Monte Carlo simulation. By providing a more complete description of resistance than previous simplified models have done while avoiding the expense of a detailed finite-element or other solid mechanics model, the method proposed here holds promise as a rapid, consistent, and accurate way to quantify wind resistance in any arbitrary wood-frame load path, with applications including insurance risk analysis, hybrid data science frameworks utilizing post-storm reconnaissance data, and estimation of hazard intensity from structural damage observations.

1. Introduction

Light wood-frame construction comprises most of the residential building inventory in the United States. The recognized vulnerability of wood-frame structures to extreme wind loads, such as those that attend hurricanes and tornadoes, and a wide variability in building performance resulting in part from differences in construction practices and building code requirements in different jurisdictions have motivated ongoing research efforts toward understanding precisely how and why wood-frame structural failures occur under wind loads and how damage can be effectively and economically mitigated in future wind events. An important product of these efforts has been the development of methods for probabilistic modeling of wind performance (Ellingwood and Tekie, 1999). At the level of individual structural components, previous probabilistic studies of wood-frame buildings have considered performance of roof sheathing (Lee and Rosowsky, 2005) and uncorrelated performance of roof sheathing and roof-to-wall connections (Rosowsky and Cheng, 1999; Ellingwood et al., 2004; Standohar-Alfano and van de Lindt, 2016). Systemlevel analysis of partial load path models composed of roof sheathing and roof-to-wall connections has been conducted in terms of building performance expectations (van de Lindt and Dao, 2009) and combined fragility functions based on defined damage states (Amini and van de Lindt, 2014; Masoomi et al., 2018), and modeling of a load path as a series system of roof sheathing, roof-towall, and wall-to-foundation connections has been carried out in terms of a failure event tree (Standohar-Alfano et al., 2017).

The methodologies of these studies share several features in common. Each develops a wind load model in terms ASCE 7 wind load parameters, similarly to the approach presented by Ellingwood and Tekie (1999). Dead load statistics for some building components, like roof cover materials, are drawn from reference design values in ASCE 7 (e.g. Masoomi *et al.*, 2018).

However, dead load statistics associated with the weight of structural members, such as the cumulative dead load acting at roof-to-wall connections, seem to be arbitrarily defined rather than based on an accounting of the true weight of components and members tributary to the point of interest. Rosowsky and Cheng (1999), for example, supply a mean dead load of 0.72 kPa (15 psf) at the roof-to-wall connection in their analysis, representing the distributed weight of the entire roof system; although the authors qualify this as an assumption that is intended to be representative of the baseline structures selected for this study, the same assumed roof-to-wall dead load has nevertheless carried through as a reference value to a number of later studies, including Ellingwood et al. (2004), Amini et al. (2014), Masoomi et al. (2018), and others. Additionally, uplift capacity statistics in these studies are based on benchmark ultimate capacities obtained from uplift tests such as those of Mizzell (1994) for roof sheathing and Reed et al. (1997) for various roof-to-wall connectors. Alternatively, other studies have employed analytical or semi-analytical resistance models for specific wood-frame connections (Guha and Kopp, 2014; Enajar et al., 2023) or developed finite-element models of partial load paths (Satheeskumar et al., 2017; Stevenson et al., 2019; Fusco and Zhu, 2023). Although these more sophisticated modeling approaches offer attractive advantages for purposes of capturing system-level interactions and nonlinear behavior, their relative complexity and computational expense make them difficult to generalize into a modeling framework that is both holistic in its analysis of every load path connection and able to accommodate a wide array of wood-frame load paths.

The studies noted in the preceding survey and others recognize that the wind performance of light wood-frame buildings is fundamentally a function of the wind loads acting on the structure and the resistance of the building elements to those loads. Yet these components — loads and resistance — are also themselves highly variable with numerous sources of epistemic and aleatory

uncertainties that combined contribute to the high variability in performance so often observed in post-windstorm reconnaissance studies. For example, Roueche et al. (2017) estimated based on field studies after the 2011 Joplin, Missouri tornado that the interquartile range for the probability of a single-family home experiencing at least major roof structure damage was approximately 22 m/s (50 mph). Therefore, in order to elucidate more precisely the causal factors driving windstorm performance, it may be advantageous to purposefully focus separately on the load factors and resistance factors that ultimately determine the final performance of such structures. Since the selection of a wind load model presupposes mean roof height, roof shape and slope, and other factors related to building geometry and subsequently aerodynamics, the results of reliability analyses, which necessarily consider both load and resistance, are applicable to one or a few structural archetypes. Moreover, though the record of wood-frame structural performance studies represents a general progression toward system-level analyses involving more detailed resistance models, simplified load paths composed of two or three connections necessarily capture only the uncertainty in structural resistance associated with those connections. These limitations underscore the potential contribution of a new modeling approach, focused exclusively on resistance at present, that is capable of closely estimating the full uncertainty in structural resistance of any wood-frame load path without regard to the aerodynamics of the surrounding structure, so as to account only for the variability in wind performance that arises from construction practices and other properties intrinsic to the structural load path itself.

This study presents such a framework for modeling wind uplift resistance of load paths in light wood-frame construction, for the primary purpose of evaluating relative structural resistance in various vertical load path configurations. It is noted at the outset that the proposed methodology models uplift resistance in the absence of lateral loads. Modeling the combined effects of shear or

out-of-plane loads simultaneously with uplift is not deemed essential at this stage since the intent of this framework is not necessarily to predict resistance in absolute terms, but rather to provide a rational and consistent way to classify different vertical load path configurations by relative wind vulnerability for use in broader risk assessment models. Representing the load path by an equivalent load chain of series components, wind uplift resistance is evaluated using a Monte Carlo-based method informed by a user-defined input parameter set containing load path structural and material properties and system-level decision parameters. Rather than considering a simplified load path consisting of only a few connections, the intent behind this modeling approach is to account for every connection in the load path that contributes to uplift resistance (stemming from extensive reconnaissance studies performed by the second author), both the more commonly studied connections as well as those that have received less attention. Further, the framework is adaptable to various load paths composed of arbitrary assemblages of structural members and is organized such that multiple cases considering different sets of connections and other load path attributes are straightforwardly evaluated. The method is demonstrated for two archetypal load paths, within which several cases are considered to assess the relative effects of different construction practices and retrofits on vertical load path performance.

2. Vertical Load Path Resistance

The vertical load path refers to the set of structural members and connections through which wind uplift forces are transferred from the roof to the foundation. The vertical load paths of two single-story wood-frame buildings are depicted in **Figure 1**, illustrating the set of connections that contribute to wind uplift resistance and associated failure modes A subset of these load path connections and failure modes is shown in **Figure 2**. Every member and connection in the load path resists some part of the total uplift force; system resistance of the load path is thus limited by the member or connection that is weakest relative to its demand. Accordingly, the approach proposed in this study is a first-order analytical model of uplift resistance that approximates system behavior by modeling the load path as an equivalent load chain composed of links in series and computing system resistance as the resistance of the weakest point in the chain. For computational simplicity, the modeling approach is not intended to account for non-linear behavior resulting from ductile failure of connections or load sharing.

2.1. Capacity Models

Mean capacities are computed from design equations provided in applicable design specifications, adjusted to ultimate strength levels. For nailed connections in wood, capacities are based on design formulas prescribed in the *National Design Specification for Wood Construction* (2018). Withdrawal capacity of smooth-shank nails is computed according to **Equation 1**:

$$C_{w} = K_{w} K_{F} G^{5/2} d(l-t)$$
 (1)

where C_w is the withdrawal capacity of a single nail, G is wood specific gravity, d is nail shank diameter, l is nail shank length, and t is the thickness of the side member that is nailed to the main

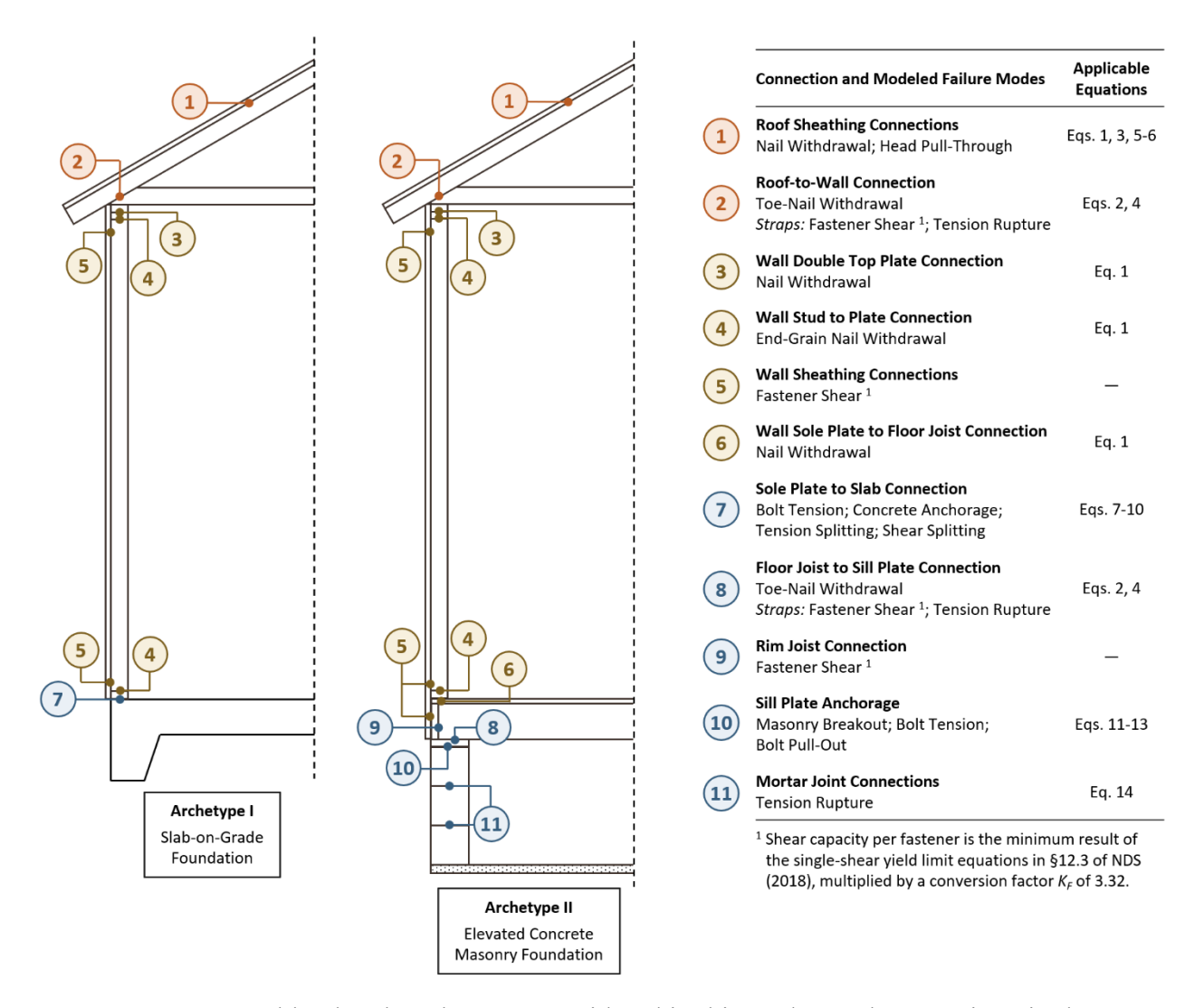


Figure 1. Structural load path archetypes considered in this study. Archetype I is a single-story home on a slab-on-grade foundation; Archetype II is built on a concrete masonry stem wall or pier foundation. Load path connections and typical failure modes under uplift forces are noted in the legend; equation numbers correspond to capacity model equations defined in Sec. 2.1.

member. K_F is the prescribed LRFD format conversion factor of 3.32, and K_w is an empirical constant equal to 9.51 MPa (1,380 psi). For nail withdrawal from wood end-grain, which has no design capacity per NDS, the result of **Equation 1** is multiplied by an end-grain capacity reduction factor K_{end} , modeled by a truncated normal distribution with a mean of 0.625 and COV of 0.10 and bounded between 0.50 and 0.75, based on estimated ratios of side-grain to end-grain withdrawal



Figure 2. Post-storm damage observations involving (a) toe-nailed roof-to-wall connection failure, (b) stud wall failure, (c) removal of wall framing from floor framing, (d) loss of rim joist, (e) failure of floor joist to sill plate connection, and (f) partial collapse of concrete masonry stem wall.

strength reported in the *Wood Handbook* (FPL, 2021). Withdrawal capacity of toe-nails is based on **Equation 2**:

$$C_{wt} = K_{toe} K_w K_F G^{5/2} d(l - (l/3) \cos 30^\circ)$$
 (2)

for a smooth-shank nail of length l driven at an angle of 30° and a toe-nail factor K_{toe} of 0.67 in accord with NDS. For ring-shank nails, withdrawal capacity of perpendicular-to-grain and toe-nailed connections is computed from **Equations 3-4** respectively:

$$C_{wr} = K_{wr} K_F G^2 d(l-t)$$
(3)

$$C_{wrt} = K_{toe} K_{wr} K_F G^2 d(l - (l/3) \cos 30^\circ)$$
 (4)

where the empirical constant K_{wr} is 12.4 MPa (1,800 psi). For roof sheathing panels, uplift capacity is based on the minimum of nail withdrawal capacity, from **Equation 1** or **3**, and nail head pull-through capacity C_{pt} , computed from **Equation 5**:

$$C_{pt} = K_F K_{pt} \pi d_h G_s^2 \tag{5}$$

where d_h is nail head diameter, G_s is sheathing specific gravity, and K_{pt} is an empirical coefficient equal to $4.76t_s$ N/mm (690 t_s lb/in.) for sheathing thicknesses $t_s \le 2.5d_h$ and equal to $11.9d_h$ N/mm (1,725 d_h lb/in.) for $t_s > 2.5d_h$. In this framework, roof sheathing panel failure is defined by failure of the fastener with the greatest effective tributary area A_{eff} , computed from **Equation 6** according to an empirical relationship developed in NAHB (2002):

$$A_{eff} = 0.10A_g^2 + A_g \tag{6}$$

where the geometric tributary area A_g is the product of the roof framing member spacing and the fastener field spacing. Further, roof sheathing nail capacities are subject to an overdriving factor F_{od} to capture the effect of overdriven nails, where $(1 - F_{od})$ represents the depth of nail head embedment into the roof sheathing as a fraction of sheathing thickness. In the probabilistic results of this study, F_{od} is modeled by a truncated normal distribution with a mean of 0.85 and a COV of 0.20, bounded between 0.70 and 1, and is applied as a multiplicative reduction factor to nail head

pull-through capacity C_{pt} in **Equation 5** and to through-member thickness t in **Equation 1** or 3, reflecting a slight increase in nail embedment depth into the framing member.

Lateral capacity C_l of nailed connections is computed as the minimum single-shear lateral design value across all yield modes considered in NDS, adjusted by the format conversion factor K_F of 3.32. This capacity model is used for wood-to-wood lateral connections as well as for wood-to-metal lateral connections such as hurricane tie roof-to-wall connections. For hurricane ties, lateral capacity is computed for a single fastener and multiplied by the number of fasteners connecting the tie to each framing member; tension capacity of the tie is also checked based on its ultimate tensile strength and minimum cross-sectional area.

Uplift capacity C_s of anchor-bolted connections to concrete slab-on-grade foundations is based on the limits states of bolt tension and concrete anchorage capacity in accord with ACI 318-14, *Building Code Requirements for Structural Concrete* (2014), given by **Equations 7-8**:

$$C_{sy} = (\pi/4)d_b^2 f_{bt} (7)$$

$$C_{sc} = 4\pi l_b^2 \sqrt{f_c'} \tag{8}$$

where d_b is nominal bolt diameter, f_{bt} is bolt ultimate tensile strength, l_b is bolt embedment length, and f'_c is concrete compressive strength in psi. Capacity of wall sole plates through which anchor bolts are installed is also evaluated with respect to shear and tension perpendicular to grain according to **Equations 9-10**:

$$C_{sv} = 2.88 A_v f_v (9)$$

$$C_{st} = 2.70 \frac{4I_p f_t}{d_p (b_p - d_w)} \tag{10}$$

where b_p and d_p are the cross-sectional width and depth of the sole plate, d_w is the diameter of the washer installed in the bolted connection, and shear strength f_v and tension strength f_t perpendicular-to-grain are functions of wood species. The coefficients correspond to the LRFD format conversion factors prescribed in NDS for shear and tension. A_v represents the area over which uplift-generated shear stresses act in the sole plate; in the analysis results presented in Sec. 3.2, A_v is assumed to be the product of bolt spacing s_b and sole plate depth d_p . The area moment of inertia I_p is computed about the longitudinal axis of the sole plate over some effective length. The effective length is at most equal to the bolt spacing s_b , though this is likely unconservative; taking the effective length as some fraction of s_b seems more appropriate. (The effective length is taken as $0.33s_b$ in the results of Sec. 3.2.) Thus the capacity C_s of a slab-on-grade embedded anchor bolt connection is taken as the minimum result of **Equations 7-10**, which together consider splitting of the sole plate due to shear or weak-axis flexure, along with breakout and tension failure of the anchor bolt.

For wood-frame walls constructed atop concrete masonry foundations, masonry connection capacity models are drawn from TMS 402-22, *Building Code Requirements for Masonry Structures* (2022). For anchor bolt connections in masonry, uplift capacity C_a is taken as the minimum result of **Equations 11-13**, which represent the limit states of masonry tension breakout, anchor tension failure, and anchor pull-out respectively.

$$C_{ab} = 4\pi l_b^2 \sqrt{f_m'}$$
 (11)

$$C_{ay} = (\pi/4)d_b^2 f_{bt} \tag{12}$$

$$C_{ap} = 1.50 f_m'(e_b d_b) + 300\pi (l_b + e_b + d_b) d_b$$
 (13)

where f_m is masonry compressive strength in psi and e_b is anchor bolt hook length. The masonry breakout capacity C_{ab} is adjustable by a multiplicative reduction factor to model instances of partial grouting in the cell containing the anchor bolt. Tensile capacity C_m of mortar joints is computed from **Equation 14**:

$$C_m = A_n f_r \tag{14}$$

where the mortar rupture strength f_r is a function of mortar type and the net joint area per foot A_n is a function of grouting condition, whether fully grouted or face-shell grouted. In the latter case, A_n is assigned a value equal to the area of contacting face-shells, scalable by a reduction factor to account for areas of grout that are either missing or damaged prior to wind loading.

2.2. System Resistance

Capacities computed using **Equations 1-14** are expressed in terms of force per unit length of wall by normalizing with respect to connection spacing s. Capacities of parallel connections, which are connections that cannot fail independently of one another, are summed to construct a load chain of series components. The wall stud-plate connection, for example, is controlled by the relatively weak failure mode of end-grain nail withdrawal, but it resists uplift in parallel with the wall sheathing connection that overlaps the stud-plate joint. Accordingly, the capacity of the composite connection is modeled as the sum of the withdrawal capacity C_w of the stud-plate end-nails and the lateral capacity C_l of the sheathing panel edge nails driven into the wall plate.

The uplift resistance *R* of component *i* in the series load chain is expressed in **Equation 15** as the sum of ultimate capacity and cumulative dead load:

$$R_{i} = \sum_{j=1}^{k} \frac{N_{j}C_{ij}}{s_{j}} + \sum_{m=1}^{i} \frac{D_{m}}{s_{m}}$$
 (15)

where ultimate capacity C is summed over k parallel connections, with each connection composed of N/s fasteners per unit length of wall, and the dead load D is summed over all members m located above component i in the load path. As with capacities, member dead loads are quantified per unit length of wall; for out-of-plane members, such as roof rafters, trusses, joists, and subflooring, dead loads are based on a tributary depth d_i equal to member span measured to the nearest interior support. System resistance is then the minimum of all series resistances R as in **Equation 16**:

$$R_{SVS} = \min R \tag{16}$$

2.3. Model Evaluation

Application of the uplift resistance model to specific buildings proceeds in three stages. First, a load path archetype is selected that matches the assemblage of structural members present in the target building. The two load paths depicted in **Figure 1**, which are intended to be representative of common residential construction in the southeastern United States, are the archetypes considered in the results presented in Sec. 3.2. Second, the input parameter set corresponding to the selected archetype is defined by assigning a probability distribution to every parameter that influences uplift resistance in any component in the load path. Inputs are grouped into three classes:

1. Structural parameters describe the basic attributes of the load path structural members, such as size, spacing, and wood species of framing members. These parameters are

modeled by discrete distributions with one or more possible values, which may be weighted or unweighted; for example, the species used for wall framing in one scenario might be set to Southern pine in three out of four realizations and to spruce-pine-fir in all others.

- 2. Material parameters include the strength properties and unit weights of building materials, such as wood shear strength, concrete compressive strength, and framing specific gravity. Material parameters are modeled by continuous distributions, and some are coupled with upstream parameters; for example, the framing wood species selected in each realization sets the distributions of specific gravity and shear and tensile strength in keeping with the properties of that species, from which the values of the material parameters are then sampled.
- 3. Connection parameters are discrete variables that define the various ways load path connections may be configured, such as whether the roof-to-wall connection is made with toe-nails only or with a hurricane tie, or whether wall sheathing overlaps the upper top plate. These parameters also encompass the attributes that can vary within each connection configuration, such as length and diameter of fasteners, number of fasteners, and bolt embedment length. As with the structural parameters, configuration and attribute distributions can be weighted according to expected relative frequencies of occurrence. In the analytical results of Sec. 3.2, the connection parameter set has been informed both by fastener schedules prescribed in the *International Building Code* (2018) and field observations by the authors. Roof-to-wall connections, for instance, are assumed to be composed of a toe-nailed connection matching one of the rafter-to-top-plate schedules

prescribed in Table 2304.10.1 of IBC (2018), which in some realizations is reinforced by an H2.5 or H8 hurricane tie, based on observations during post-windstorm damage surveys, especially in high-wind regions.

The load path structural, material, and connection parameter sets applicable to the archetypes shown in **Figure 1** are summarized in **Tables 1-3**. Finally, after defining the input parameter set, system-level uplift resistance is evaluated by Monte Carlo simulation. Each load path realization is formed by sampling from the input parameter distributions; sampled inputs are supplied to **Equations 1-14** as applicable for the various connections in the load path, and system resistance is subsequently estimated via **Equations 15** and **16**.

 Table 1. Load Path Structural Parameters

Parameter	Definition	Distribution Type	Purpose in Model
Component Materials	Material types used for components and cladding, including roof cover, wall cladding, and floor finishes.	Discrete	Contributes to dead load.
Framing Wood Species	Wood species of framing members; can be assigned to roof, wall, and floor framing independently.	Discrete	Affects withdrawal [Eqs. 1-4] and lateral capacity of fasteners and wood member capacity in shear and tension [Eqs. 9-10]; affects dead load by determining wood density.
Member Sizes	Dimensional measurements of rafters, joists, plates, studs, sheathing, and other structural members in the load path.	Discrete	Affects through-member thickness t in withdrawal [Eqs. 1, 3], pull-through [Eq. 5], and lateral capacity equations; affects mortar joint area A_n [Eq. 14]; affects dead load by determining structural member volume.
Member Spacings, s	Spacing of rafters, studs, joists, and other repetitive structural members, measured center-to-center along wall length.	Discrete	Normalizes capacity of connections involving repetitive members and normalizes dead load contributed by repetitive members [Eq. 15].
Roof Slope	Roof angle relative to horizontal.	Deterministic ^a	Affects dead load contributed by roof structure.
Sheathing Type	Type of sheathing panels used; assigned to roof and wall sheathing independently.	Discrete	Affects pull-through capacity in roof sheathing [Eq. 5], lateral capacity in wall sheathing, and dead load by determining sheathing density.
Tributary Depth, d_t	Span from exterior wall to nearest interior support; can be assigned to roof and floor systems independently.	Deterministic ^a	Affects dead load contributed by out- of-plane members, such as rafters and joists.

^a For purposes of computing dead load, a value must be assigned to this parameter; however, because the wind uplift load is itself a function of this parameter, it is not treated probabilistically in this study.

 Table 2. Load Path Material Parameters

Parameter	Symbol	Definition	Applicable Equations
Component Weights	_	Unit weights of components and cladding corresponding to the material types defined in Table 1 .	_
Framing Specific Gravity ^a	G	Specific gravity of framing members corresponding to the various wood species defined in Table 1 .	Eqs. 1-4
Sheathing Specific Gravity	G_s	Specific gravity of sheathing panels corresponding to sheathing types defined in Table 1 .	Eq. 5
Anchor Bolt Tensile Strength	f_{bt}	Ultimate tensile strength of anchor bolts embedded in concrete or masonry.	Eqs. 7, 12
Concrete Compressive Strength	f'_c	Compressive strength of concrete in slab-on-grade foundations.	Eq. 8
Wood Shear Strength	f_{v}	Shear strength of wood members perpendicular to grain corresponding to the wood species defined in Table 1 .	Eq. 9
Wood Tensile Strength	f_t	Tensile strength of wood members perpendicular to grain corresponding to the wood species defined in Table 1 .	Eq. 10
Masonry Compressive Strength	f'_m	Compressive strength of concrete masonry in concrete stem wall or pier foundations.	Eqs. 11, 13
Mortar Rupture Strength	f_r	Rupture strength of mortar corresponding to the mortar types defined in Table 3 .	Eq. 14

^a In each load path realization, G is sampled from the selected distribution independently at each connection as applicable.

 Table 3. Connection Parameters

Connection	Configurations	Connection Attributes	Applicable Archetypes
Roof Sheathing		Nail length and diameter; nail type; nail edge and field spacing.	I and II
Roof-to-Wall	(a) Toe-nails only; (b) toe-nailed with hurricane strap.	Toe-nail length, diameter, and type; number of toe-nails; type of hurricane strap, such as H2.5 or H8.	I and II
Wall Double Top Plate	(a) Face-nails only; reinforced by (b) hurricane strap, (c) overlapping wall sheathing, or (d) both.	Face-nail length and diameter; number and spacing of nails.	I and II
Wall Stud to Plate		Nail length and diameter; number of nails.	I and II
Wall Sheathing	(a) Overlaps lower top plate and sole plate only; overlaps (b) upper top plate, (c) rim joist, or (d) both. ^a	Nail length and diameter; nail edge spacing.	I and II
Wall Sole Plate to Concrete Slab		Anchor bolt diameter, embedment length, and spacing; washer diameter.	I
Wall Sole Plate to Floor Joist		Nail length and diameter; number of nails.	II
Floor Joist to Sill Plate	(a) Toe-nails only; (b) toe-nailed with hurricane strap.	Toe-nail length, diameter, and type; number of toe-nails; type of hurricane strap, such as H2.5 or H8.	II
Rim Joist to Floor Joists		Nail length and diameter; number of nails.	II
Sill Plate Anchorage	(a) Anchor bolts are installed in fully grouted cells; (b) cells are partially grouted. ^b	Anchor bolt diameter, embedment length, hook length, and spacing.	II
Mortar Joints	(a) Concrete masonry unit cells are fully grouted; (b) only face-shells are grouted. ^b	Mortar type: affects rupture strength.	II

^a Configurations (c) and (d) apply only to Archetype II.
^b Configuration (b) activates a multiplicative reduction factor on the applicable capacity equation, as described in Sec. 2.1.

3. Results

As a way to validate the use of NDS-based capacity models, the results of a component-level comparison between experimental uplift capacities and modeled ultimate uplift capacities are first presented for selected load path connections. Probabilistic model results for various load path cases are then presented based on the structural archetypes in **Figure 1**.

3.1. Comparison to Experimental Uplift Capacities

A selection of mean experimental failure pressures from past roof sheathing uplift studies, primarily based on a summary compiled by Datin et al. (2011), is compared to modeled uplift resistances in **Table 4**. These test results are representative of various combinations of typical nail sizes, framing wood species, sheathing types and thicknesses, and nail spacings. Common smoothshank nails are used in most test configurations, with ring-shank nails considered in a few series. In each case, the modeled ultimate capacity is based on the lesser of (1) the nail withdrawal capacity computed from Equation 1 or 3 depending on shank type and (2) the nail head pullthrough capacity computed from Equation 5. The minimum result of these equations, which is the controlling capacity of a single fastener, is divided by the critical effective tributary area defined by **Equation 6**, where the framing member spacing is 0.61 m (24 in.). The resulting critical fastener capacity is then added to the sheathing unit weight to obtain the modeled ultimate resistance. For this set of results, experimental resistance is under-predicted by as much as 54% and overpredicted by as much as 62%, with an average prediction error of about +1%. A deterministic overdriving factor F_{od} of 0.90 is applied to the modeled capacities in **Table 4** to account for a mild effect due to overdriven nails; for factors of 1 and 0.80, the prediction error bounds are [-48%, +57%] with an average of +3% and [-59%, +67%] with an average of -5% respectively. On average across these test series, the model appears to provide a reasonable estimate of the mean ultimate

capacity of roof sheathing panels. Pearson correlation coefficients are given in **Table 5** for all model variables with respect to the prediction error, in both relative and absolute terms, suggesting a moderate under-prediction bias associated with larger nails and ring-shank nails, and possibly with framing specific gravity and sheathing thickness to a lesser degree. Aside from these potential correlations and the systemic modeling error they may indicate, much of the scatter in the prediction error appears to be a consequence of aleatory uncertainty in the experimental results themselves, driven by differences in test protocols, limited numbers of samples in some instances, and the natural variability of wood properties.

A selection of mean experimental uplift failure loads for various roof-to-wall connections are presented in Table 6 alongside corresponding modeled ultimate capacities. The studies cited in Table 6 encompass a range of typical connector configurations and framing wood species. All are laboratory tests that applied monotonic uplift loading to specimens constructed of new lumber, except Shanmugam et al. (2009) who conducted in situ testing of rafter-to-wall connections in aged lumber under cyclic loading and Edmonson et al. (2012) who tested new lumber specimens as well as laboratory-built specimens of lumber reclaimed from the same source as in Shanmugam et al. (2009). Most studies considered smooth-shank common or box toe-nails; Morrison and Kopp (2011) and Alhawamdeh and Shao (2020) provide benchmark capacities for deformed-shank toenails. Additionally, three studies tested connections made with hurricane ties, either as the sole connector or in conjunction with toe-nails. Observed variability in the results of similar test series is partly a consequence of differences in test methodology but primarily reflects the inherent uncertainty in toe-nail withdrawal capacity due to variability in wood density and toe-nail embedment depth, which is a function of toe-nail angle and the height at which toe-nails are installed relative to the wall top plate. Modeled toe-nail withdrawal capacities under-predict these

Table 4. Comparison of Roof Sheathing Connection Uplift Resistances

Reference	Nail Type and Spacing ^a	Framing Specific Gravity ^b	Sheathing Type ^c	Samples	COV	Mean Experimental Resistance	Modeled Ultimate Resistance	Error
						kPa (psf)	kPa (psf)	
Cunningham	C-6-6:12	0.50	P-15/32	1	_	2.63 (55)	2.91 (61)	+11%
(1993)	C-8-6:12	0.50	P-15/32	1	_	6.22 (130)	3.08 (64)	-51%
	C-6-6:12	0.50	O-7/16	1		3.11 (65)	3.00 (63)	-4%
	C-8-6:12	0.50	P-5/8	1	_	5.03 (105)	4.10 (86)	-18%
	C-6-6:6	0.50	P-15/32	1	_	5.75 (120)	6.26 (131)	+9%
	C-8-6:6	0.50	P-5/8	1	_	10.44 (218)	8.84 (185)	-15%
	RS-8-6:6	0.50	P-5/8	1		19.01 (397)	8.84 (185)	-54%
Mizzell	C-6-6:12	0.42	P-15/32	4	0.09	1.20 (25)	1.94 (40)	+62%
(1994)	C-8-6:12	0.42	P-15/32	10	0.11	2.92 (61)	2.92 (61)	-0.1%
	C-8-6:6	0.42	P-15/32	10	0.16	5.12 (107)	6.28 (131)	+23%
	C-8-6:6	0.42	P-19/32	10	0.28	5.51 (115)	5.96 (125)	+8%
	C-8-6:6	0.42	O-19/32	10	0.27	3.69 (77)	5.96 (125)	+62%
Jones	C-8-6:12	0.49	O-19/32	10	0.28	4.17 (87)	3.95 (82)	-5%
$(1998)^d$	C-8-6:12	0.49	P-15/32	9	0.17	3.83 (80)	3.08 (64)	-20%
Sutt (2000)	C-8-6:12	0.55	P-1/2	7	0.09	3.78 (79)	3.28 (69)	-13%
	C-8-6:12	0.55	O-7/16	7	0.15	3.21 (67)	4.04 (84)	+26%
Datin et al.	$C-6-6:12^f$	0.55	O-1/2	15	0.22	3.56 (74)	4.54 (95)	+28%
$(2011)^{e}$	C-6-6:12	0.55	O-1/2	5	0.16	2.94 (62)	3.67 (77)	+25%
	C-6-6:6	0.55	O-1/2	5	0.27	5.18 (108)	7.91 (165)	+53%
	C-8-6:12	0.55	O-1/2	15	0.12	6.20 (129)	4.63 (97)	-25%
	C-8-6:8	0.55	O-1/2	15	0.12	8.38 (175)	7.31 (153)	-13%
	C-8-6:6	0.55	O-1/2	15	0.10	9.83 (205)	10.01 (209)	+2%
	RS-8-6:12 ^g	0.55	O-1/2	25	0.15	8.10 (169)	5.13 (107)	-37%
	RS-8-6:8 ^g	0.55	O-1/2	15	0.17	10.35 (216)	8.11 (169)	-22%
	RS-8-6:6 ^g	0.55	O-1/2	13	0.07	12.08 (252)	11.11 (232)	-8%
							verage Error	+1%

^a Nail nomenclature: C and RS signify common smooth-shank nails and ring-shank nails respectively; the first number denotes a nail size of 6d or 8d, where, unless noted otherwise, a 6d nail is 2.87 mm (0.113 in.) diam. by 50.8 mm (2.00 in.) in length with a nail head diam. of 6.76 mm (0.266 in.) and an 8d nail is 3.32 mm (0.131 in.) diam. by 63.5 mm (2.50 in.) in length with a nail head diam. of 7.14 mm (0.281 in.); the numbers separated by a colon are the edge and field spacing in inches.

^b Specific gravities taken from Table 12.3.3A of NDS (2018) based on reported wood species of framing in test specimens.

^c Sheathing nomenclature: P and O signify plywood and OSB respectively; the fractional number indicates thickness in inches.

^d Framing wood species in this study was an unspecified combination of Southern yellow pine and spruce-pine-fir.

^e Nail head diameter not reported for second and third series in this study; assumed to be 6.76 mm (0.266 in.) in the model result.

f Nail shank length reported as 60.3 mm (2.38 in.).

g Nail head diameter reported as 7.95 mm (0.313 in.).

Table 5. Roof Sheathing Parameter Correlation Coefficients

Parameter	Correlation Coefficients				
	Based on Relative Error	Based on Absolute Error			
Nail Shank Diameter	-0.52	-0.38			
Nail Head Diameter	-0.46	-0.34			
Nail Shank Length	-0.49	-0.35			
Nail Shank Type ^a	-0.45	-0.63			
Framing Specific Gravity	-0.31	-0.16			
Sheathing Specific Gravity b	+0.19	+0.22			
Sheathing Thickness	-0.17	-0.34			
Nail Field Spacing	-0.13	+0.05			

^aBinary variable for smooth-shank or ring-shank.

experimental results by as much as 43% and over-predict by as much as 62%. As with roof sheathing, no clear relationship can be discerned between the modeled and experimental capacities for toe-nailed connections, but inasmuch as the modeled capacities fall within an envelope formed by upper and lower-bound test results, the comparison suggests that the NDS-based modeling approach provides a reasonable toe-nailed connection capacity estimate for use within the larger load path resistance framework. As for hurricane ties, the model over-predicts the experimental results both of Reed *et al.* (1997) and of the new-lumber test series in Edmonson *et al.* (2012) by about 15%, while the aged-lumber test series results in Edmonson *et al.* (2012) are over-predicted by 44% for an H10 as the only connector and by 29% for a combined toe-nail and H10 connection. The result found by Alhawamdeh and Shao (2020) is over-predicted by 134%, though the mean experimental capacity of this series is strikingly weak relative to the capacity levels obtained in earlier studies. Moreover, a statistical analysis by Edmonson *et al.* (2012) concluded that individual capacities of toe-nails and hurricane ties are additive for purposes of estimating the uplift capacity of the composite roof-to-wall connection.

^b Specific gravities taken as 0.42 for plywood and 0.50 for OSB.

Table 6. Comparison of Roof-to-Wall Connection Uplift Capacities

Reference	Connectors	Specific Gravity	Samples	COV	Mean Experimental Capacity	Modeled Ultimate Capacity	Error
					kN(lb.)	kN(lb.)	
Reed et al.	(3) 8d Common ^a	0.55 ^c	16	0.23	1.91 (430)	1.85 (416)	-3%
(1997)	(3) 8d Common + H2.5 ^b	0.55^{c}	16	0.11	8.47 (1,900)	9.68 (2,176)	+15%
Jones	(3) 8d Common	0.55^{c}	20	0.25	1.91 (429)	1.85 (416)	-3%
(1998)	(3) 8d Common	0.42^{c}	20	0.23	1.53 (343)	0.94 (212)	-38%
Cheng	(2) $16d \text{ Box }^d$	0.417	10	0.09	1.13 (255)	0.89 (200)	-21%
(2004)	(2) 16d Box	0.419	16	0.27	1.56 (350)	0.90 (203)	-42%
	(2) 16d Box	0.454	10	0.15	1.48 (332)	1.10 (248)	-25%
	(3) 8d Box ^e	0.427	10	0.15	1.10 (248)	0.85 (191)	-23%
	(2) 16d Common ^f	0.452	12	0.16	2.30 (518)	1.31 (294)	-43%
	(2) 16d Box	0.539	14	0.19	2.83 (637)	1.69 (381)	-40%
	(2) 16d Box	0.546	11	0.13	2.74 (615)	1.75 (393)	-36%
	(2) 16d Box	0.565	14	0.21	2.60 (584)	1.90 (428)	-27%
	(2) 16d Box	0.563	14	0.16	2.69 (637)	1.89 (424)	-30%
Shanmugam	(2) 16d Common	0.55^{c}	81	0.36	1.52 (341)	2.12 (477)	+40%
et al. (2009)	(3) 16d Common	0.55^{c}	19	0.28	1.97 (442)	3.19 (716)	+62%
Morrison and	(3) Twisted-Shank	0.50^{c}	63	0.21	2.80 (629)	3.60 (810)	+29%
Kopp (2011) ^g	(2) Twisted-Shank	0.50^{c}	16	0.24	1.90 (427)	2.40 (540)	+26%
	(2) Twisted-Shank	0.50^{c}	16	0.22	2.20 (495)	2.40 (540)	+9%
Edmonson	(2) 16d Common	0.55^{c}	10	0.21	2.98 (670)	2.11 (474)	-29%
et al. (2012) ^h	H10 ⁱ	0.55^{c}	10	0.13	12.2 (2,733)	14.1 (3,168)	+16%
	H10	0.55^{c}	13	0.17	9.77 (2,198)	14.1 (3,168)	+44%
	(2) 16d Common + H10	0.55^{c}	7	0.10	12.6 (2,830)	16.2 (3,642)	+29%
Alhawamdeh and Shao (2020)	(3) Ring-Shank ^j	0.50^{c}	5	0.07	1.91 (430)	1.89 (426)	-1%
	(3) Ring-Shank + H2.5	0.50 ^c	5	0.08	3.90 (877)	9.12 (2,051)	+134%
			Avera	ge Erroi	for Toe-Nailed	Connections	-10%
				Avera	ge Error for All	Connections	+2%

^aToe-nails 3.32 mm (0.131 in.) diam. by 63.5 mm (2.50 in.) length.

^b 18-gauge galvanized steel tie fastened with (5) nails 3.32 mm (0.131 in.) diam. by 38.1 mm (1.50 in.) length into the rafter and (5) nails 3.32 mm (0.131 in.) diam. by 63.5 mm (2.50 in.) length into the wall top plate.

^c Estimate based on reported wood species of test specimens.

^d Toe-nails 3.43 mm (0.135 in.) diam. by 88.9 mm (3.50 in.) length.

^e Toe-nails 2.87 mm (0.113 in.) diam. by 63.5 mm (2.50 in.) length.

^f Toe-nails 4.09 mm (0.161 in.) diam. by 88.9 mm (3.50 in.) length.

g Toe-nails described as 12d twisted-shank, here taken to be 3.43 mm (0.135 in.) diam. by 82.6 mm (3.25 in.) length. The second and third cases in this study are for two toe-nails on one side of the connection and one toe-nail on each side, respectively.

^h The second case listed for this study used new Southern pine specimens; the other three used reclaimed Southern pine.

¹⁸⁻gauge galvanized steel plate fastened with two groups of (9) nails 3.32 mm (0.131 in.) diam. by 38.1 mm (1.50 in.) length.

Toe-nails were 2.87 mm (0.113 in.) diam. by 60.3 mm (2.38 in.) long ring-shank nails driven approximately at 45°.

Beyond roof sheathing and roof-to-wall connections, for which experimental uplift failure data are readily available, Standohar-Alfano *et al.* (2017) offer benchmark wall-to-foundation connection capacities based on uplift load testing of four stud wall specimens, two with reinforcing stud-plate ties and two without ties. The specimens without ties characteristically failed by withdrawal of end-nails from the studs; the specimens with stud-plate ties instead failed by splitting of the sole plate around the anchor bolts. Similarly, pull-out tests of anchor bolts embedded in concrete conducted by Nilforoush *et al.* (2017) provide reference anchorage capacities for bolted connections in slab foundations. Representative modeled capacities are compared to these benchmark capacities in **Table 7**. Though the reference experimental results drawn from the two preceding studies are determined from only two or three specimens per test series, they illustrate that experimental capacities for stud-plate withdrawal, sole plate splitting, and concrete anchorage failures can be approximated by supplying reasonable input values to the respective capacity models.

3.2. Analysis of Load Path Resistance

Probabilistic output from the modeling framework takes the form of **Figures 3-4**, which depict five distinct load path cases for each of the two archetypes illustrated in **Figure 1**. In all cases, the number of simulations n is 50,000. The results of each modeled case are conveyed in three plots. The left-hand plot reports the uplift resistance of each component in the series load chain. Mean resistance, computed as the sum of mean ultimate capacity and mean cumulative dead load, is represented by the two-segment bars; uncertainty bars indicating the median and interquartile range are superimposed on the bar chart. The center plot reports how likely each series component is to be weakest in the load chain. A connection with a weakest-link probability of 40%, for example, is expected to be the location where system failure initiates in 40% of outcomes.

Table 7. Representative Modeled Capacities for Wall-to-Slab-Foundation Failure Modes

Reference	Failure Mode	Controlling Capacity Model	Modeled Capacity	Mean Experimental Capacity
Standohar-Alfano	End-Nail Withdrawal	$3.32 K_{end} K_w G^{5/2} d(l-t)$ [Eq. 1]	1.97 kN/m (135 lb/ft.) ^a	1.90 kN/m (130 lb/ft.)
et al. (2017)	Sole Plate Splitting	$2.70 \frac{4I_p f_t}{d_p (b_p - d_w)}$ [Eq. 10] ^b	2.76 kN/m (189 lb/ft.) ^c	2.80 kN/m (190 lb/ft.)
		Concrete Slab Depth	a a	Mean Experimental Capacity
		33 cm (1.08 ft.)		324 kN (72.8 k)
Nilforoush <i>et al</i> .	Concrete Anchorage	44 cm (1.44 ft.) $4\pi l_b^2 \sqrt{f_c'}$ [Eq. 8] e		339 kN (76.3 k)
(2017) ^d	Failure	$4\pi t_b \sqrt{J_c}$ [Eq. 6] 66 cm (2.17 ft.)		376 kN (84.4 k)
		44 cm (1.44 ft.)		484 kN (108.7 k)

^a Result of Eq. 1 for two 16d common nails, 4.11 mm (0.162 in.) diam. by 88.9 mm (3.50 in.) length, a specific gravity G of 0.40, and an end-grain factor K_{end} of 0.60, normalized by a stud spacing of 0.41 m (16 in.).

The right-hand plot provides the normalized distribution of system resistance, based on the resistance of the weakest series component. The median uplift resistance in each case is reported for ease of comparison between cases.

^b Eqs. 7 and 9 also apply in this case but do not control over wood splitting due to tension.

^c Result of Eq. 10 for an estimated wood tension strength f_t of 0.32 MPa (47 psi), a washer diameter d_w of 38.1 mm (1.50 in.), sole plate depth and breadth of 38.1 mm (1.50 in.) and 88.9 mm (3.50 in.), a bolt spacing s_b of 1.83 m (72 in.), and a moment of inertia I_p of 281 cm⁴ (6.75 in.⁴) based on an effective length equal to $s_b/3$; the result is normalized by s_b .

d Comparing to the NPC and HPC test cases in this study.

^e Eq. 7 for bolt tension rupture also applies in this case but does not control due to the use of high-strength bolts in these tests.

 $[^]f$ Results of Eq. 8 for a bolt embedment length l_b of 8.66 in. (22 cm) and concrete compressive strengths f'_c of 5,947 psi (41.0 MPa), 5,642 psi (38.9 MPa), 5,816 psi (40.1 MPa), and 11,850 psi (81.7 MPa); error increases with slab depth.

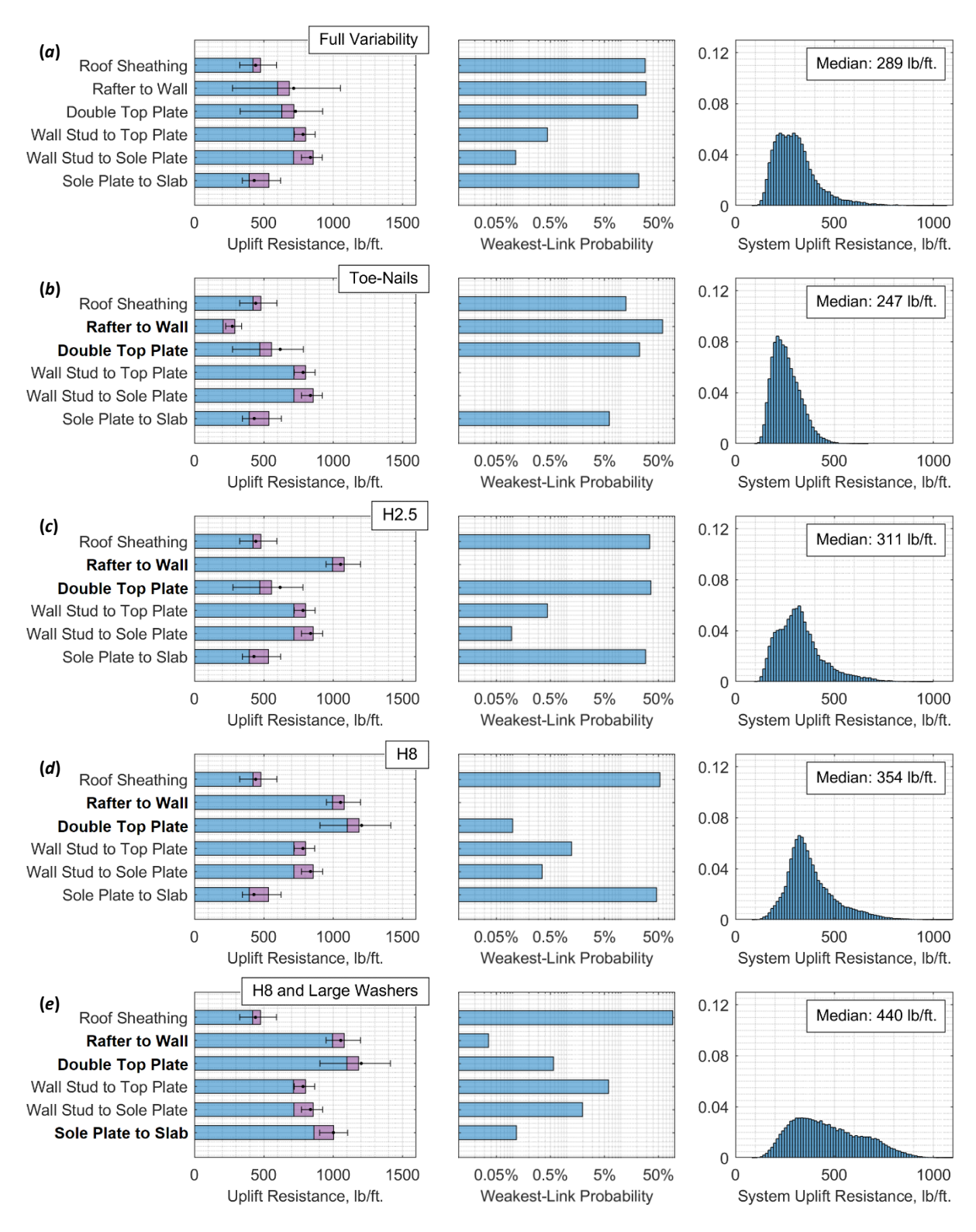


Figure 3. Resistance model results for selected cases based on Archetype I, in which (a) is a reference case, (b) includes only toe-nailed roof-to-wall connections, (c) includes only H2.5 hurricane-tie roof-to-wall connections, (d) includes only H8 hurricane-tie connections, and (e) includes only H8 hurricane ties and large-diameter washers at the wall-to-slab connection. [Conversion: 1 lb/ft. = 14.59 N/m]

The results in Figure 3 for an Archetype I home on a slab-on-grade foundation illustrate the effect of progressive strengthening of weak connections in the load path. Figure 3(a) depicts a reference case representing "full variability" with respect to the possible connection configurations and attribute values. Specifically, the reference case assumes that (1) the roof-towall connection may be composed of toe-nails only or toe-nails in conjunction with a hurricane tie, (2) the hurricane tie, if present, may be either an H2.5 or an H8, and (3) the washer diameter at the wall-to-slab connection can vary between 2.54 cm (1 in.) and 7.62 cm (3 in.), with all outcomes equally likely. Subsequent cases evaluate the effects of restricting these connection parameters to certain outcomes. The center plot in Figure 3(a) indicates a relatively even distribution of likely failure initiation points in the reference case: the roof sheathing, rafter-towall, double top plate, and sole-plate-to-slab connections are each responsible for system failure in 20-30% of realizations. In **Figure 3(b)** the roof-to-wall connection is always toe-nailed. The rafter-to-wall uplift resistance decreases accordingly, as does that of the double top plate, which is still sometimes reinforced by overlapping wall sheathing but is no longer strengthened by an H8 hurricane tie, which reaches to the lower top plate. In this scenario about 60% of system failures are expected to begin at the rafter-to-wall connection, reflecting the relative weakness of toe-nailed connections to uplift; median uplift resistance of the load path as a whole decreases by 15% from the reference case. The roof-to-wall connection is upgraded to an H2.5 hurricane tie in **Figure 3**(c), which effectively eliminates the rafter-to-wall connection as a possible failure point; median system resistance rises about 8% relative to case (a), with almost all system failures attributable to roof sheathing, double top plate, or wall-to-slab failure in nearly equal proportions. The roof-towall connection is further upgraded to an H8 tie in Figure 3(d), which provides rafter-to-wall capacity comparable to an H2.5 and also substantially reinforces the double top plate in all realizations. This makes top plate separation the limiting failure mode in only 0.1% of instances and increases median system resistance by 22% relative to case (a). Lastly, in **Figure 3**(e) the wall-to-slab connection is assigned only large washers 7.62 cm (3 in.) in diameter, sharply reducing the likelihood of wood splitting around the anchor bolt. Once these improvements have been made, median system resistance is 52% greater than in the baseline full-variability case, and removal of roof sheathing is the controlling failure in more than 90% of realizations, facilitating the top-down failure sequence that is ideal for wind. Since the roof sheathing capacity in all cases in **Figure 3** is sampled from a uniform distribution of 6d and 8d smooth-shank and ring-shank nails and field spacings of 15.2, 20.3, and 30.5 cm (6, 8, and 12 in.), the most direct way to strengthen the load path further would be to constrain the sheathing connection options to stronger fastener schedules.

The second group of results in **Figure 4**, for an Archetype II home on a concrete masonry pier foundation, illustrates the significance of several parameters that tend not to be captured in post-windstorm field surveys. **Figure 4**(*a*) represents "full variability" in the load path parameters, as in the reference case of **Figure 3**(*a*). Specifically, the **Figure 4**(*a*) reference case assumes that (1) the wood species of all framing members may be any of four common species, (2) wall sheathing may overlap both top plates or only the lower top plate, and (3) wall sheathing may be continuous across the wall-to-floor connection or reach only to the sole plate, with all outcomes equally likely. In **Figure 4**(*b*) the framing wood species is limited to Southern yellow pine, which is the densest of the four species considered in the reference case and thus enhances the mean capacity of all wood-to-wood connections in the load path. Relative failure probabilities are slightly re-ordered but not substantially changed; median system resistance rises by 24% compared to case (*a*). In **Figure 4**(*c*), the wood species constraint is removed, and the sheathing overlap of the upper top plate is active in all realizations; compared to the reference case in (*a*), the probability

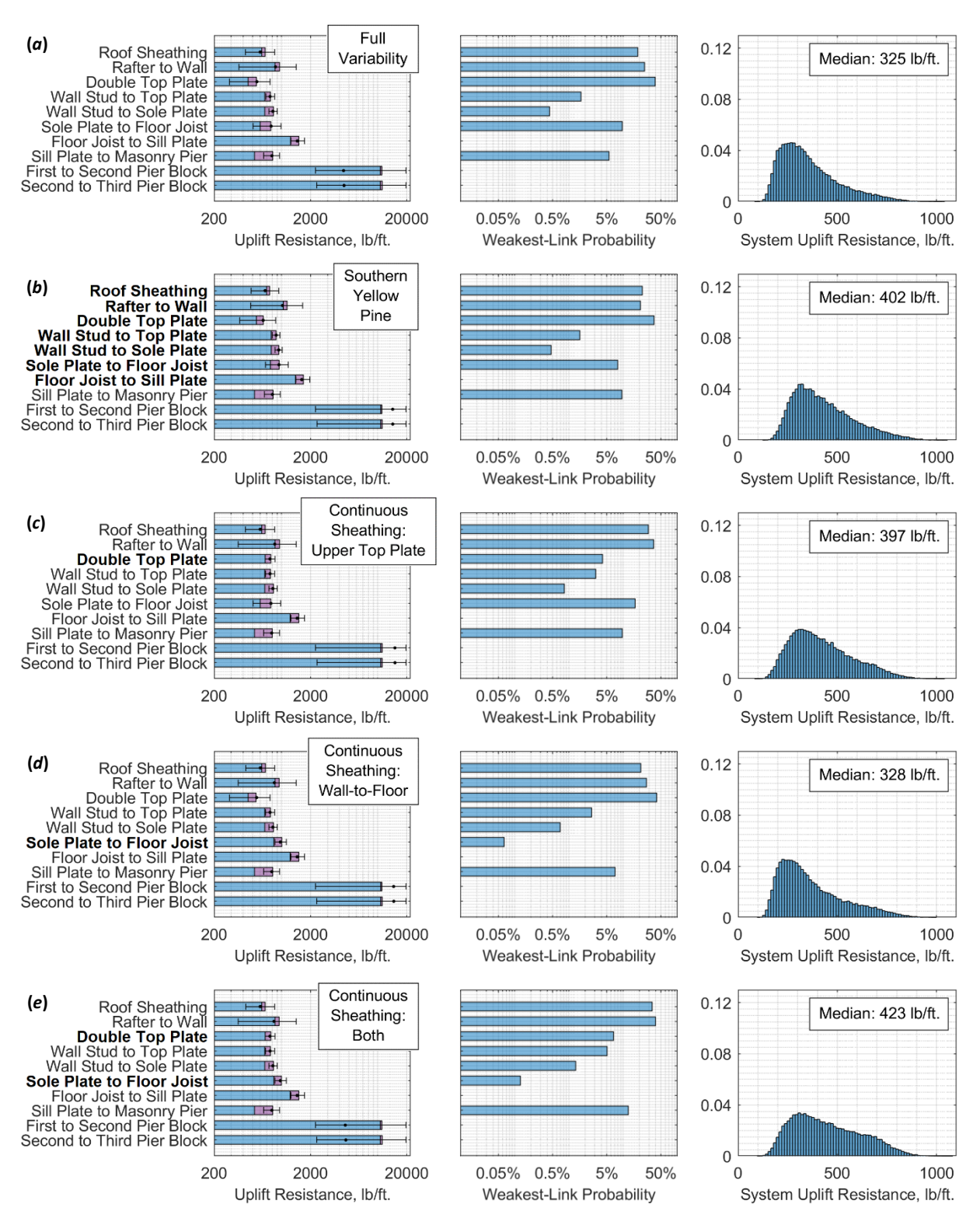


Figure 4. Resistance model results for selected cases based on Archetype II, in which (a) is a reference case, (b) limits framing wood species to Southern yellow pine, (c) enforces the sheathing overlap of the double top plate in all instances, (d) enforces the sheathing overlap of the wall-to-floor connection in all instances, and (e) enforces both sheathing overlaps. Left-hand bar graphs are plotted on a logarithmic scale for readability. [Conversion: 1 lb/ft. = 14.59 N/m]

of failure initiation at the double top plate connection is reduced by a factor of ten to around 4%, with a 22% rise in median system resistance. On the other hand, unconstraining the upper top plate overlap but enforcing the overlap of the sole-plate-to-floor connection as in **Figure 4(d)** attenuates the failure initiation rate for that connection to less than 0.1% but does not substantially improve system resistance since the three weaker links in case (a) remain unaddressed. Both sheathing overlaps are enforced in all realizations in **Figure 4(e)**, raising median system resistance by 30% relative to the reference case. These comparisons underscore the usefulness of capturing such construction details as sheathing nail placement and wood species whenever these details are accessible.

Application of the framework to post-windstorm reconnaissance is further demonstrated in Figures 5-6. In Figure 5, a reference case for Archetype I is again established by seeking to retain full variability in the most influential load path parameters. The same assumptions made for the reference case in Figure 3(a) also apply to Figure 5(a), with the addition of variability in roof rafter spacing, edge spacing of wall sheathing nails, and slab anchor bolt spacing. Field data obtained from several similarly constructed homes in Lake Charles, Louisiana impacted by Hurricane Laura, all of which correspond to Archetype I, are then entered into the model to generate results tailored to this specific load path case. Observations include a typical roof rafter spacing of 0.41 m (16 in.), toe-nailed roof-to-wall connections, a typical anchor bolt spacing of 1.52 m (5 ft.), non-oversized anchor bolt washers, and Southern yellow pine as the typical framing wood species. The new model input reduces the system resistance interquartile range by 39%, from 2.17 kN/m (148 lb/ft.) to 1.33 kN/m (91 lb/ft.), representing the reduced uncertainty in resistance associated with these field observations.

A similar reference case for Archetype II is considered in **Figure 6(a)**, representing a generalized case of a single-story home on a concrete masonry stem wall foundation. **Figure 6(b)** presents updated results in light of field observations recorded for a number of such homes in Cookeville, Tennessee after the tornado outbreak of March 3, 2020, including typical roof truss and floor joist spacings of 0.61 m (24 in.) and 0.41 m (16 in.) respectively, a 3:1 ratio of H2.5 hurricane tie roof-to-wall connections versus toe-nailed-only connections, a typical wall framing wood species of spruce-pine-fir, sheathed double top plate connections, a typical anchor bolt spacing of 1.22 m (4 ft.), and ungrouted stem wall cells. Supplying these data to the model reduces the system resistance interquartile range by 16%, from 3.06 kN/m (210 lb/ft.) to 2.56 kN/m (176 lb/ft.).

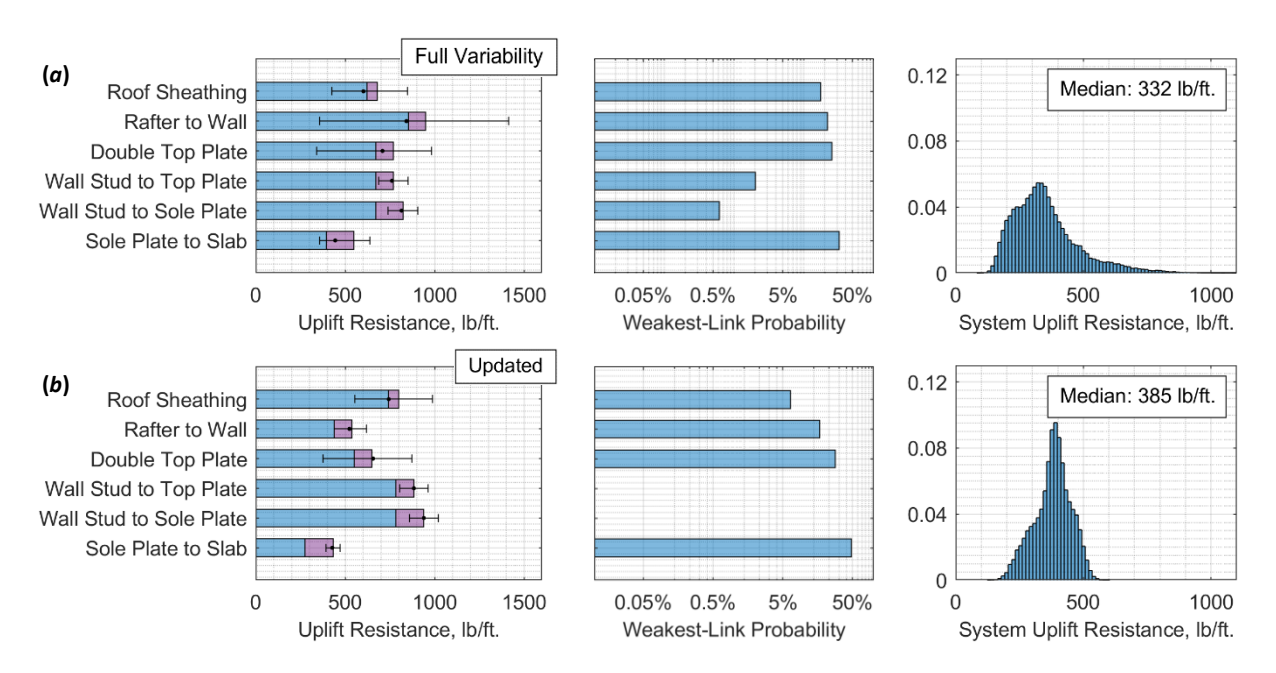


Figure 5. (a) Model results for a generalized case of Archetype I based on common construction practices. (b) Updated model results informed by field data collected for a typical load path observed in several homes in Lake Charles, Louisiana impacted by Hurricane Laura in August, 2020. [Conversion: 1 lb/ft. = 14.59 N/m]

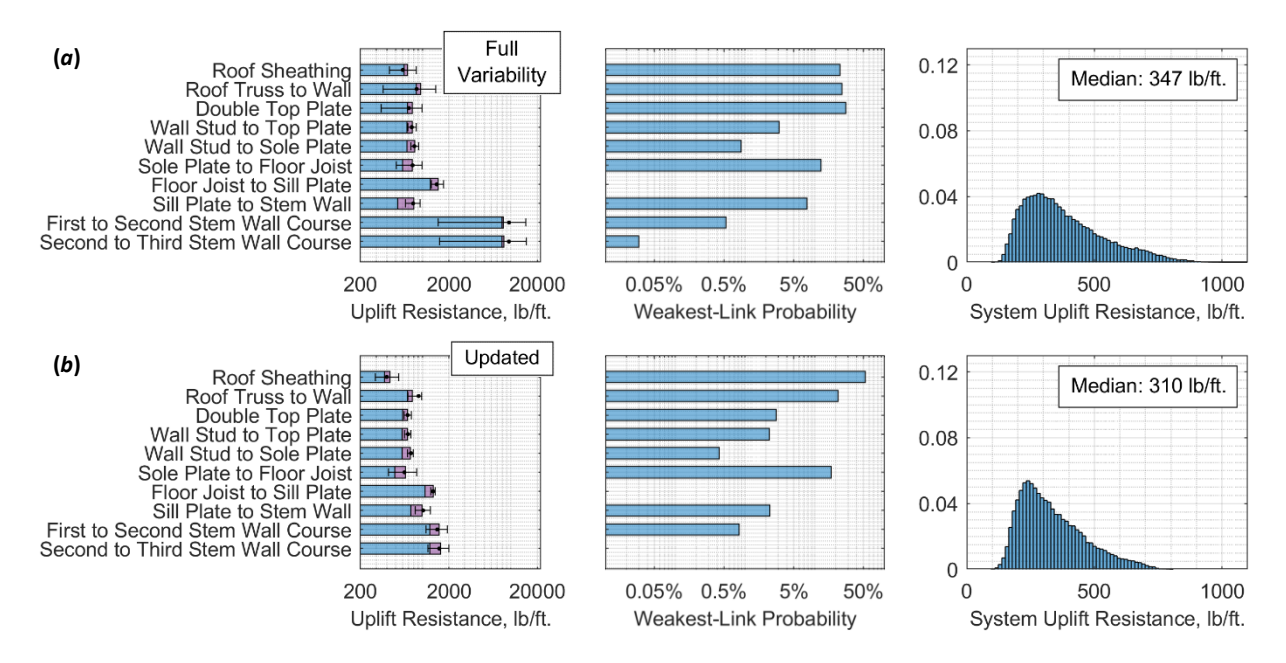


Figure 6. (a) Model results for a generalized case of Archetype II based on common construction practices. (b) Updated model results informed by field data collected for a typical load path encountered during field assessments in Cookeville, Tennessee after the tornado outbreak of March 3, 2020. Left-hand bar graphs are plotted on a logarithmic scale for readability. [Conversion: 1 lb/ft. = 14.59 N/m]

Such case studies as those presented in **Figures 5** and **6** illustrate the benefits of using the proposed modeling framework to evaluate the anticipated resistance of various load path configurations directly observed in the field relative to baseline scenarios. This could have practical relevance, for example, in the use of the Enhanced Fujita Scale (Mehta, 2013), which is used to estimate the intensity of tornadoes based on observed damage. A key element of the EF Scale method requires that personnel in the field select a wind speed to associate with the observed damage from within a range of possible wind speeds by accounting for, among other factors, weaker-than-typical or stronger-than-typical construction practices. This framework provides a rational basis for evaluating this relative resistance when, for example, a home may have hurricane straps at the roof-to-wall connections (generally indicative of stronger-than-typical construction) yet only use small washers with the anchor bolts at the sole plate. Further, this framework provides a rational basis to demonstrate the importance of a complete load path in wind mitigation. While

so much attention is typically focused on individual elements (e.g., anchor bolt, hurricane strap), the framework demonstrates that the benefits of such improvements may be marginal without strengthening the complete load path.

4. Conclusions

The modeling approach described herein appears promising as an efficient and readily adaptable method to evaluate relative wind uplift resistance in wood-frame load paths. The approach has sought to build on previous probabilistic studies by accounting for every vertical load path connection and considering the variability of every attribute that affects uplift resistance, thereby capturing the full uncertainty in structural resistance intrinsic to the load path under study. Adopting established design equations as the basis for connection capacity models avoids the computational expense of high-fidelity solid mechanics models and allows for large sets of load path cases to be evaluated in short order. Ultimate capacities based on design provisions generally agree with experimental capacities for selected load path connections, though further testing is warranted to determine benchmark capacities of connections for which no experimental data are presently available. System-level uplift testing of archetypal load paths would serve to validate the equivalent series load-chain approach and better consider the non-linearities of the load path. As the proposed framework does not model the effects of lateral forces in conjunction with uplift, further model development to account for shear and out-of-plane loads, and ultimately a broadening of the framework to model lateral load path resistance of elements like diaphragms and shear walls, would also be beneficial.

Representing the load path as a set of series components provides a consistent way to assess disparities in connection strength. The unused, surplus capacity in connections that are reinforced well beyond the available capacity in other parts of the load path can be clearly seen and quantified.

Load paths can similarly be graded with respect to a target failure sequence; a top-down failure sequence, for example, in which loss of roof sheathing is most likely to occur first, followed by roof framing members, and so on, would be preferable in virtually every case to failure initiation at some point closer to the foundation. Future prescriptive designs for wood-frame buildings could be checked against an ideal failure sequence by applying the model in this manner. Thus, although the proposed framework is not intended to form the basis of a design procedure, it can nevertheless be used to inform design and retrofitting decisions to optimize load path performance.

Application of the framework to a series of specific load path cases also demonstrates its potential as an uncertainty quantification tool in assessing the system-level effect of various load path modifications. Such a use carries value for insurance risk analysis as a method to evaluate whether insurance incentives offered for certain strengthened connections or other retrofits are commensurate with the reduced risk of damage realized by those improvements. Further, from the perspective of post-windstorm reconnaissance, the framework can process any number of field observations collected for a wind-impacted structure and quickly generate a structural resistance distribution tailored to that load path, with implications for wind hazard intensity estimation. However, since the present framework only considers uplift resistance, it may overpredict the failure wind speed in situations where significant lateral wind loads act in combination with uplift wind loads on elements of the structural load path. The framework can also facilitate, via sensitivity studies, recommendations for what perishable data should be prioritized for collection in the field based on the relative influence various factors (e.g., wood species, fastener dimensions) have on the uplift resistance distributions.

Acknowledgments

This work was sponsored in part by the National Science Foundation under CAREER research grant CMMI-1944149. Any opinions, findings, and conclusions or recommendations expressed in this material are those of the authors and do not necessarily reflect the views of the National Science Foundation.

References

- Alhawamdeh, B., and X. Shao. 2020. "Uplift Capacity of Light-Frame Rafter to Top Plates Connections Applied with Elastomeric Construction Adhesives." *J. Mater. Civ. Eng.*, 32 (5): 04020078. https://doi.org/10.1061/(ASCE)MT.1943-5533.0003152.
- American Concrete Institute. 2014. *Building Code Requirements for Structural Concrete*. ACI 318-14.
- American Wood Council. 2018. National Design Specification for Wood Construction.
- Amini, M. O., and J. W. van de Lindt. 2014. "Quantitative Insight into Rational Tornado Design Wind Speeds for Residential Wood-Frame Structures Using Fragility Approach." *J. Struct. Eng.*, 140 (7): 04014033. https://doi.org/10.1061/(ASCE)ST.1943-541X.0000914.
- Cheng, J. 2004. "Testing and Analysis of the Toe-Nailed Connection in the Residential Roof-to-Wall System." For. Prod. J., 54 (4): 58–65.
- Cunningham, T. P. 1993. *Roof Sheathing Fastening Schedules for Wind Uplift*. Tacoma, Washington, United States: American Plywood Association.
- Datin, P. L., D. O. Prevatt, and W. Pang. 2011. "Wind-Uplift Capacity of Residential Wood Roof-Sheathing Panels Retrofitted with Insulating Foam Adhesive." *J. Archit. Eng.*, 17 (4): 144–154. https://doi.org/10.1061/(ASCE)AE.1943-5568.0000034.
- Edmonson, W. C., S. D. Schiff, and B. G. Nielson. 2012. "Behavior of Light-Framed Wood Roof-to-Wall Connectors Using Aged Lumber and Multiple Connection Mechanisms." *J. Perform. Constr. Facil.*, 26 (1): 26–37. https://doi.org/10.1061/(ASCE)CF.1943-5509.0000201.
- Ellingwood, B. R., D. V. Rosowsky, Y. Li, and J. H. Kim. 2004. "Fragility Assessment of Light-Frame Wood Construction Subjected to Wind and Earthquake Hazards." *J. Struct. Eng.*, 130 (12): 1921–1930. https://doi.org/10.1061/(ASCE)0733-9445(2004)130:12(1921).
- Ellingwood, B. R., and P. B. Tekie. 1999. "Wind Load Statistics for Probability-Based Structural Design." *J. Struct. Eng.*, 125 (4): 453–463. https://doi.org/10.1061/(ASCE)0733-9445(1999)125:4(453).
- Enajar, A., A. Nassef, and A. El Damatty. 2023. "Reliability of Toe-Nail Connections in Gable Roof Houses Under Uplift Wind Loads." *Eng. Struct.*, 274: 115199. https://doi.org/10.1016/j.engstruct.2022.115199.

- Forest Products Laboratory. 2021. *Wood Handbook: Wood as an Engineering Material*. 546. General Technical Report. Madison, Wisconsin: Forest Products Laboratory, United States Forest Service, United States Department of Agriculture.
- Fusco, G., and J. Zhu. 2023. "Personalized Vulnerability Assessment of Customized Low-Rise Wood-Frame Residential Structures Under Hurricane Wind Loads: A Flexible Scenario-Based Simulation Approach." *ASCE-ASME J. Risk Uncertainty Eng. Syst., Part A: Civ. Eng.*, 9 (3): 04023023. https://doi.org/10.1061/AJRUA6.RUENG-1037.
- Guha, T. K., and G. A. Kopp. 2014. "Storm Duration Effects on Roof-to-Wall-Connection Failures of a Residential, Wood-Frame, Gable Roof." *J. Wind Eng. Ind. Aerodyn.*, 133: 101–109. https://doi.org/10.1016/j.jweia.2014.08.005.
- International Code Council. 2018. International Building Code.
- Jones, D. T. 1998. "Retrofit Techniques Using Adhesives to Resist Wind Uplift in Wood Roof Systems." M.S. Thesis. Clemson, South Carolina, United States: Clemson University.
- Lee, K. H., and D. V. Rosowsky. 2005. "Fragility Assessment for Roof Sheathing Failure in High Wind Regions." *Eng. Struct.*, 27 (6): 857–868. https://doi.org/10.1016/j.engstruct.2004.12.017.
- van de Lindt, J. W., and T. N. Dao. 2009. "Performance-Based Wind Engineering for Wood-Frame Buildings." *J. Struct. Eng.*, 135 (2): 169–177. https://doi.org/10.1061/(ASCE)0733-9445(2009)135:2(169).
- Masonry Society. 2022. Building Code Requirements for Masonry Structures. TMS 402-22.
- Masoomi, H., M. R. Ameri, and J. W. van de Lindt. 2018. "Wind Performance Enhancement Strategies for Residential Wood-Frame Buildings." *J. Perform. Constr. Facil.*, 32 (3): 04018024. https://doi.org/10.1061/(ASCE)CF.1943-5509.0001172.
- Mehta, K. C. 2013. "Development of the EF-Scale for Tornado Intensity." *J. Disaster Res.*, 8 (6): 1034–1041. https://doi.org/10.20965/jdr.2013.p1034.
- Mizzell, D. P. 1994. "Wind Resistance of Sheathing for Residential Roofs." M.S. Thesis. Clemson, South Carolina, United States: Clemson University.
- Morrison, M. J., and G. A. Kopp. 2011. "Performance of Toe-Nail Connections Under Realistic Wind Loading." *Eng. Struct.*, 33 (1): 69–76. https://doi.org/10.1016/j.engstruct.2010.09.019.

- National Association of Home Builders. 2002. *Roof Framing Connections in Conventional Residential Construction*. 66. United States Department of Housing and Urban Development.
- Nilforoush, R., M. Nilsson, and L. Elfgren. 2017. "Experimental Evaluation of Tensile Behaviour of Single Cast-in-Place Anchor Bolts in Plain and Steel Fibre-Reinforced Normal- and High-Strength Concrete." *Eng. Struct.*, 147: 195–206. https://doi.org/10.1016/j.engstruct.2017.05.062.
- Reed, T. D., D. V. Rosowsky, and S. D. Schiff. 1997. "Uplift Capacity of Light-Frame Rafter to Top Plate Connections." *J. Archit. Eng.*, 3 (4): 8.
- Rosowsky, D. V., and N. Cheng. 1999. "Reliability of Light-Frame Roofs in High-Wind Regions II: Reliability Analysis." *J. Struct. Eng.*, 125 (7): 734–739. https://doi.org/10.1061/(ASCE)0733-9445(1999)125:7(734).
- Roueche, D. B., F. T. Lombardo, and D. O. Prevatt. 2017. "Empirical Approach to Evaluating the Tornado Fragility of Residential Structures." *Journal of Structural Engineering*, 143 (9): 04017123. American Society of Civil Engineers.
- Satheeskumar, N., D. J. Henderson, J. D. Ginger, and C.-H. Wang. 2017. "Three-Dimensional Finite-Element Modeling and Validation of a Timber-Framed House to Wind Loading." *J. Struct. Eng.*, 143 (9): 04017112. https://doi.org/10.1061/(ASCE)ST.1943-541X.0001850.
- Shanmugam, B., B. G. Nielson, and D. O. Prevatt. 2009. "Statistical and Analytical Models for Roof Components in Existing Light-Framed Wood Structures." *Eng. Struct.*, 31 (11): 2607–2616. https://doi.org/10.1016/j.engstruct.2009.06.009.
- Standohar-Alfano, C. D., and J. W. van de Lindt. 2016. "Tornado Risk Analysis for Residential Wood-Frame Roof Damage across the United States." *J. Struct. Eng.*, 142 (1): 04015099. https://doi.org/10.1061/(ASCE)ST.1943-541X.0001353.
- Standohar-Alfano, C. D., J. W. van de Lindt, and B. R. Ellingwood. 2017. "Vertical Load Path Failure Risk Analysis of Residential Wood-Frame Construction in Tornadoes." *J. Struct. Eng.*, 143 (7): 04017045. https://doi.org/10.1061/(ASCE)ST.1943-541X.0001775.
- Stevenson, S. A., A. M. El Ansary, and G. A. Kopp. 2019. "A Practical Modelling Technique to Assess the Performance of Wood-Frame Roofs Under Extreme Wind Loads." *Eng. Struct.*, 191: 640–648. https://doi.org/10.1016/j.engstruct.2019.04.058.
- Sutt, E. G. 2000. "The Effect of Combined Shear and Uplift Forces on Roof Sheathing Panels." Ph.D. Dissertation. Clemson, South Carolina, United States: Clemson University.